Measurement-based Command and Control Radio Channel Characterization for UAVs

L. Bernadó*, D. Löschenbrand*, C. Sulzbachner†, F. Bruckmüller† T. Zemen*
*Center for Digital Safety and Security – Security & Communication Technologies,
AIT – Austrian Institute of Technology GmbH, Vienna, Austria – firstname.name@ait.ac.at
†Center for Vision, Automation and Control – Assistive & Autonomous Systems,
AIT – Austrian Institute of Technology GmbH, Vienna, Austria - firstname.name@ait.ac.at

***Abstract*—In recent years, the amount of unmanned aerial vehicle (UAV) based applications has strongly increased. In order to fly the UAVs safely, their command and control link needs a reliable and robust communication channel. A line of sight (LOS) between the UAV operator and UAV is, at the moment, an essential requirement to guarantee an error-free communication. However, even in LOS conditions, the reception of a constant signal level is not assured. In this paper, we present the results of a measurement campaign with a UAV and a drone moving on the ground that were electronically tracked with simultaneous dedicated beams at 3,2 GHz coming from a 10 element antenna array. Small software-defined-radio modules were integrated in the drones to record the strength of the received signal when moving. The instantaneous GPS coordinates of the UAV were transmitted via a 4G link to a ground station that translated them into spherical coordinates used at the antenna array side. We show that the UAV itself and its flying inclination produce around 10 dB fluctuations in the received power, even in LOS conditions, and therefore shadowing cannot be ignored.**

***Index Terms*—UAV, drones, SDR, propagation, measurements.**

I. Introduction

Unmanned aerial systems (UAS) are proliferating in usage since a couple of decades, in diverse areas such as consumer recreation, agricultural monitoring, structural inspection, military defense, aerial sensing, search and rescue, or goods delivery [1], [4]. Unmanned aerial vehicles (UAVs) operate in an already complex airspace, shared with other manned and unmanned aircrafts. As flying objects, operational commands go over a radio link. In UAVs this communication is achieved via the command and control (C2) link, operating mainly in the 2.4 GHz ISM band. Because of the dense spectrum usage in the 2.4 GHz ISM band, there is a potential of interfering with other links when controlling a UAV, which might become critical in, i.e., safe and rescue operations. Dedicated beamforming allows for a targeted transmission thus reducing unwanted and harmful interference to other devices.

A single UAV can carry out operations that would require more effort in terms of time and economic costs whilst less risks than when conducted by a human. However, a single device has some limitations, such as the payload it can carry or the area it can cover. A group of UAVs, called UAV swarm, can cope with these limitations, thus increasing the efficiency in terms of operational expenses.

There are two kinds of architectures used in UAV swarm communication: in the *infrastructure-based* architecture the ground station receives the telemetry of all UAVs in the swarm and sends the commands to each device; in the *flying ad-hoc network-based* architecture the UAVs within the swarm communicate with each other, but at least one has to be connected to an operator (ground station or satellite) [2]. Even though it is envisioned that a swarm can be fully autonomous, the truth is that a human operated ground control station is still needed. In fact, in most cases, each individual UAV is simultaneously controlled by a ground station, which receives live telemetry data from the UAVs. In this paper, we focus on the *infrastructure-based* communication architecture as it is the most commonly used in UAV swarm communication [3].

Wave propagation undergoing in ground to air (GA) communication links strongly differs from the propagation occurring in terrestrial mobile communications and therefore it is necessary to be properly modeled. Due to its tedious measurement set-up, few campaigns have been conducted in the scientific community to characterize and model the radio channel in GA, or its reciprocal air-to-ground (AG), links [4]. First measurement campaigns for AG links conducted in the C-band and L-band using manned aircrafts are provided in [6]. A more recent list published in [5] reviews a number of measurement campaigns using unmanned aircrafts, including narrowband and wideband measurements, with a dedicated section for IEEE 802.11 based UAV communications. It also devises the UAV's high mobiliy and rotation, and airframe shadowing as some of the causes for the dynamics observed in the measurements. However, none of the mentioned campaigns was considering a multiple UAV measurement setup, and only omnidirectional antennas were used at the ground station side.

In this paper, we go beyond the single UAV C2 channel characterization and design a measurement system that enables us to simultaneously measure the received power at various UAVs and track them using an electronically adaptable multi-beamformer, thus avoiding mechanical tracking.

II. Multi-beamforming antenna array

We aim at establishing dedicated and reliable links for the C2 channel with several UAVs that move simultaneously in different directions. In order to achieve that, we design a multi-beamforming antenna array.

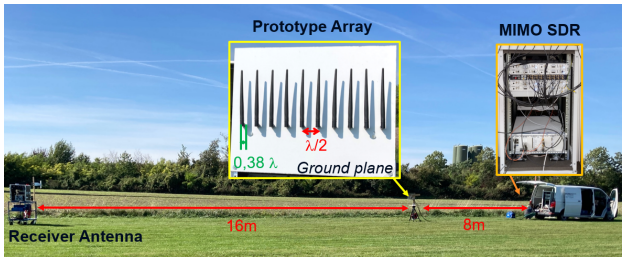

Fig. 1. Set-up for radiation pattern measurement.

A. Multi-beamforming design

We consider several global optimization techniques to solve a multidimensional non-linear optimization problem with the goal of synthesizing a multi-beam pattern. The design constrains are: (i) maximum gain value in the intended directions, (ii) 20° beamwidth in the intended directions, and (iii) otherwise the lowest possible gain in all other directions. To solve that, we evaluated the performance of multi-beamformers, in terms of cost function and run time, using particle swarm optimization, dual annealing, differential evolution and linearly-constrained minimum variance (LCMV) methods. The LCMV optimization method turned out to be the most efficient one delivering the best performance in terms of cost function and run time while meeting the specified optimization conditions.

The LCMV method, commonly used in acoustics arrays, allows for multiple linear constrains and is an extension of classic distortion-free response filtering with minimal variance. The filter coefficients are adjusted based on the statistics of the output signals, and the cost function used to calculate them is the output signal variance [8].

B. Multi-beamforming simulations

We use MATLAB to simulate a linear array consisting of 10 elements spaced $\lambda/2$, with which we can create simultaneous beams directed to up to 3 directions. Note that increasing the size of the array (in number of antenna elements and dimensions over which it expands), more simultaneous beams could be achieved. Nevertheless, we keep dimensionality low which suffices our purposes for multi-beamforming with low computational complexity. We then execute the MATLAB embedded narrowband LCMV algorithm from the phased array processing toolbox, which takes into account mutual coupling effects, and obtain the weighting coefficients to be applied to each antenna element of the array to synthesize a multi-beam pattern. For the sake of a fast adapting beam steering, these coefficients are pre-calculated using simulations and stored in a look-up-table (LUT) that will be stored in the AIT software defined radio (SDR) MIMO Testbed [9] and used in a real-time implementation.

C. Antenna Prototype and Multi-beamformer Validation

For demonstration purposes, we build a prototype consisting of an array with 10 dipoles (3.5GHz 5 dBi Rubber Duck Antenna from L-com). The array is linearly mounted along the x-axis with a ground plane that extends along the z-x plane, displayed in Fig. 1 as *Prototype Antenna*. Their omnidirectional radiating properties in azimuth are adequate for our purpose, while the nulls in the dipole axes are softer than those in theoretical dipoles.

The antennas are spaced $\lambda/2$ to avoid grating lobes, and their distance to the ground plane is 0.38λ, which contributes to increase the gain in the hemisphere in front of the array.

The C2 link in UAVs uses the 2.4 GHz ISM frequency band. In order to characterize the propagation properties of this link, we need to select a different yet close enough carrier frequency for our experiments. If we conduct our experiments in the 2.4 GHz band, we will interfere with the C2 link of the UAV, which might cause the UAV to terminate its operation as the C2 link would be disabled. Therefore, we select a carrier frequency of 3.2 GHz, for which we have a legal permission of usage within the AIT premises.

D. Multi-beam pattern measurements

To validate the simulated patterns, we conducted measurements in a free-space environment at the AIT premises. Figure 1 shows the set-up for the radiation pattern measurements. The SDR equipment used to configure the array was kept inside a van, positioned 8 m away from the array to avoid unwanted reflections. The array acted as transmitter (Tx) and we used a directional patch antenna as a receiver (Rx) placed 16 m away. We then rotated the array in steps of 5°in azimuth and stored the received signal to afterwards process it and obtain the radiation pattern.

In Fig. 2 we compare the simulated radiation patterns (in blue) with the measured ones (in red) for 1-, 2- and 3-beam patterns. We observe a good agreement between simulations and measurements: the beams point towards the desired directions (marked with green dashed lines) with a half-power beamwidth (HPBW) between 10° and 20°, being wider in the measurements. Furthermore, the measured sidelobes are higher in gain (about 5 to 10 dB) because of the ground plane used in the array, which was not accounted for during the simulations. The main lobes are always, at least, 5 dB higher than the side lobes.

III. Measurements

The antenna coefficients (amplitude and phase) for the multi-beamformer are stored in the AIT SDR-MIMO testbed [9], which consists of two modules: the antenna module and the processing module, displayed in Fig. 3 at the bottom. Furthermore, we attached a light weight SDR module (HackRF One) to the UAVs to record the measured their received signal. We used two UAVs: UAV1 is a fixed wing Skywalker EVE-2000 and UAV2 is a custom X8 copter based on Rosewhite Tamara, see Fig. 3 at the top. A dipole antenna of the same type as the ones used in the array is mounted in each of the HackRF One modules.

A. Measurement Set-up

The working system is schematically depicted in Fig. 3. The two UAVs are equipped with a GPS receiver and a 4G

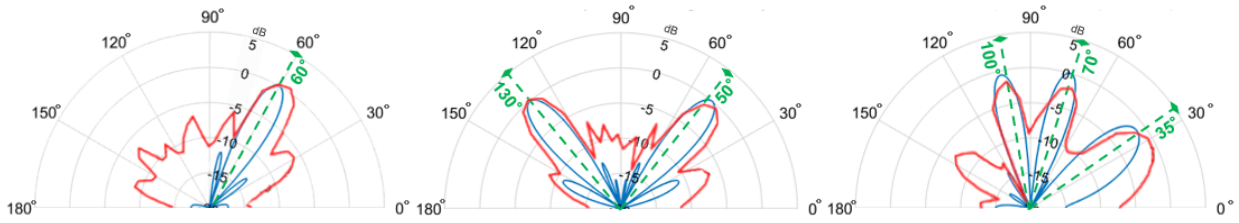

(a) 1 Beam - 60° (b) 2 Beams - 50° and 130° (c) 3 Beams - 35°, 70° and 100°

Fig. 2. Simulated (blue) and measured (red) multi-beamforming radiation patterns.

module, and they send their current position to a ground station via a 4G Link. In the ground station, the GPS positions are converted into spherical coordinates, which deliver the angle combination pointing towards the UAVs. This angle combination is transferred via a TCP to the SDR-MIMO platform, where a search in the LUT is performed to find the coefficients (amplitude and phase) that will be set to the antennas to create a pattern with the beams pointing in the direction of the UAVs. At the UAV side, the HackRF One module records the received signal, which will be matched to the current UAV position via time-stamping during the post-processing phase.

The 4G connection, together with the TCP connection used to connect the ground station to the AIT-SDR modules, introduces a latency of about 150-500 miliseconds. Considering that the maximum velocity at which the UAV moved during the tests was 20 m/s, this inaccuracy corresponds to about 3-10 m in terms of travelled distance, which translates to 2-8°, if we take into account that the UAV was always more than 70 m away from the transmitting array. Given the width of the HPBW of our multi-beamformer, we consider that inaccuracy to be negligible.

B. *Post-processing*

The data gathered in the two HackRF One modules was post-processed and matched to the position of the UAV using the internal time-stamp in the module. The post-processing involves the following steps:

1) Data smoothing: to get rid of undesired signal peaks caused in the SDR unit.

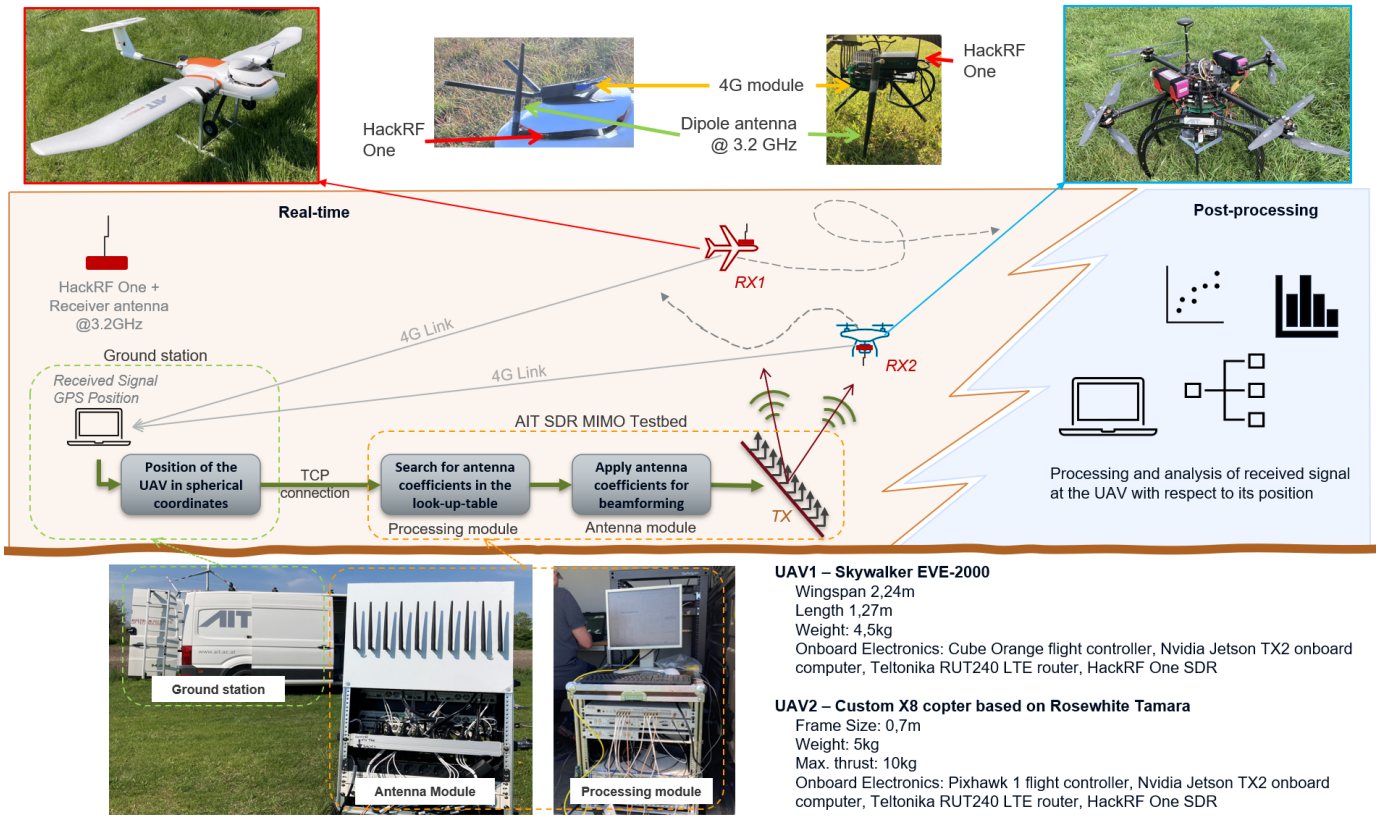

Fig. 3. Measurement set-up.

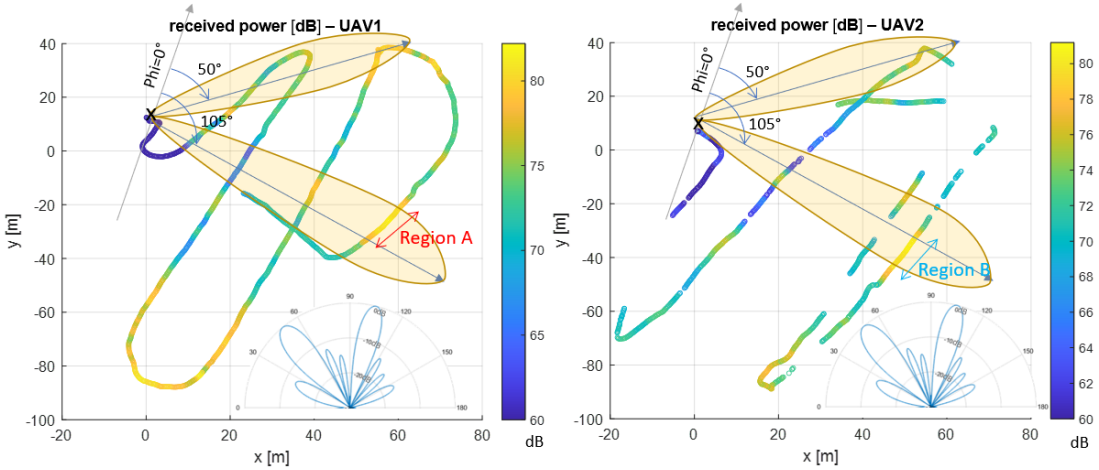

(a) Received power for UAV1

(b) Received power for UAV2

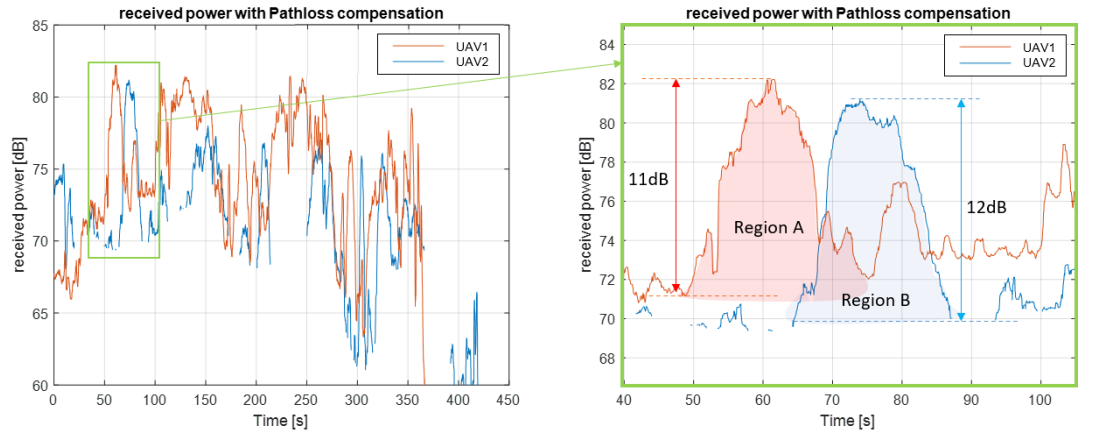

(c) Received power over time for UAV1 and UAV2 with zoomed Region A and B

Fig. 4. Test 1: Fixed beams - received power in xy coordinates and over time.

2) Noise floor removal: all values below the measured noise floor are set to NaN in order to avoid wrong data leading to misinterpretation of the results.
3) Path loss compensation: the received signal power is compensated with its free space path loss given the distance between Tx and Rx.

C. Tests Description

In order to characterize the propagation effects in the C2 link we conducted two tests:

- Test 1 - Fixed angles: the antenna coefficients are set to a constant value that creates two beams in two fixed directions, 50° and 105°.
- Test 2 - Adaptive angles: the antenna coefficients are electronically changed based on the current UAV position.

IV. Results

The experiments were carried out in a rural set-up, where line-of-sight (LOS) between the Tx (antenna array) the Rx (the UAVs) was assured and multi-path reflections were minimized, in order to isolate the propagation effects solely of the C2 link. Originally, the plan was to have both UAV flying, however, due to weather conditions, the UAVs were carried around in Test 1 and only UAV1 was flying during Test 2.

A. Test 1 - Fixed angles

The received signal along the followed trajectory is shown in Fig. 4 for the two UAVs. The areas in the trajectory where there is no data correspond to noise floor values at the Rx which are set to NaN, as explained in the previous section. Figures 4a-4b show a 2D coordinate representation of the color coded received power. Whereas Fig. 4c is a time representation of the received power.

We observe that the maxima of the received power are within the directions of the intended radiation beams (50° and 105°). However, there are areas where a strong signal is expected but low power is measured, such as in Fig. 4a at coordinates (20,-10). Conversely, there are areas with strong received signal where it is not expected, as in Fig. 4a at coordinates (0,-80).

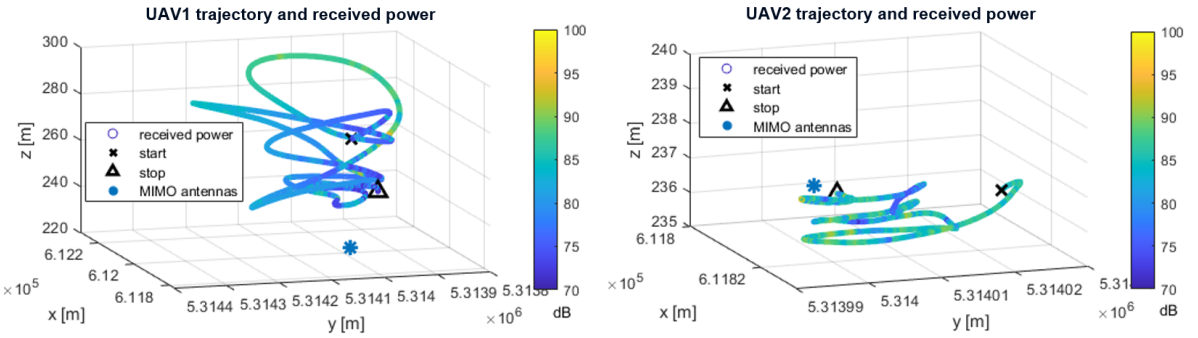

(a) Received power in UAV1.

(b) Received power in UAV2.

Fig. 5. Test 2: Adaptive beamforming - 3D representation of received power over trajectory.

These effects are manifold: first, shadowing created by the people walking with the UAVs, second, ground reflections, third, the UAV morphology and the mounting position of the antenna, and fourth, the stronger sidelobes in the radiation pattern in comparison to the simulation results (see Fig. 1, where sidelobes are measured to be between 5 and 10 dB higher than in simulations).

Furthermore, in Fig. 4c we show the performance of the received signal over time with a zoomed-out area for two regions marked as *Region A* and *Region B* in Fig. 4a, in which the UAVs cross one of the main beams. We measure a variation in the received power of up to 12 dB, which fits very well with the simulated radiation pattern for this angle combination, as shown in the bottom right corner in Fig. 4a-4b.

B. Test 2 - Adaptive angles

The recorded signal over the trajectories can be seen in Fig. 5 in a 3D representation for the two UAVs. Note that the UAV1 trajectory changes considerably along the z-axis, as it is flying, whereas the UAV2's z coordinates remain constant during the whole measurement (within GPS accuracy of 1 m), as it is being carried.

To better interpret the results, we plot the received power against time in a 2D diagram in Fig. 6, where we filled out the NaN values (when the received power is below the noise floor) using linear interpolation. Note that the straight line between 280 and 310 s in the received power for UAV2 is the result of this interpolation.

We observe a steady fluctuation within 10 dB for the received power in the UAV on the ground, and a greater variation in the received power for the flying UAV. It is noteworthy to mention that the fluctuations observed in Test 1 correlate well with the moment when the UAVs cross the main and side lobes of the generated and fixed multi-beam pattern. On the other hand, the fluctuations observed in Test 2 are from a different nature. First, note the steadiness of the received power for UAV2 (being carried at ground level). And secondly, the smooth trend of maxima and minima on top of shorter variations observed in the received power for UAV1.

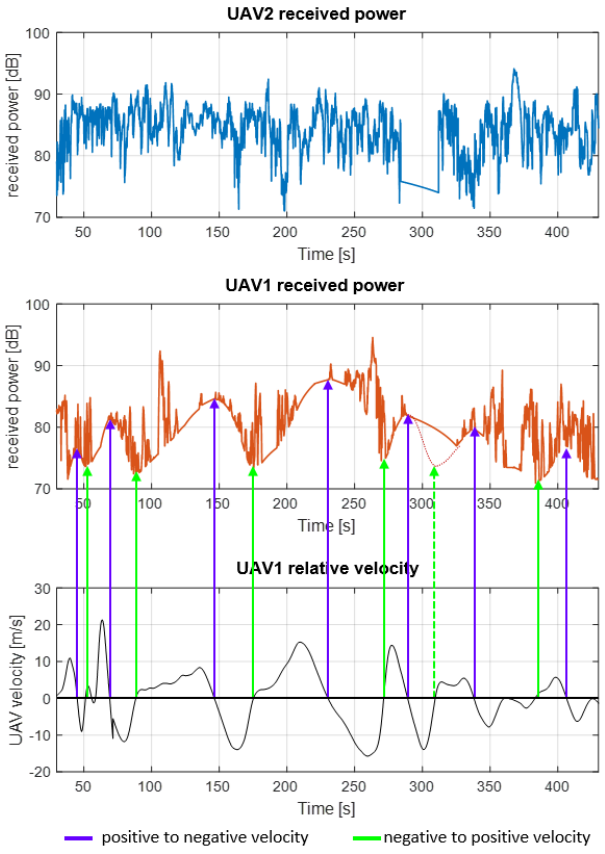

Fig. 6. Test 2: Adaptive beamforming - Received power and instantaneous velocity.

In order to find a justification for this higher power changes, we looked into the instantaneous relative velocity of the UAV1 and observed that there is a correlation between maxima and minima in the received power and the relative velocity zero crossings.

The instantaneous relative velocity is calculating using the instantaneous distance of the UAV relative to the antenna array. When the speed transitions from negative to positive

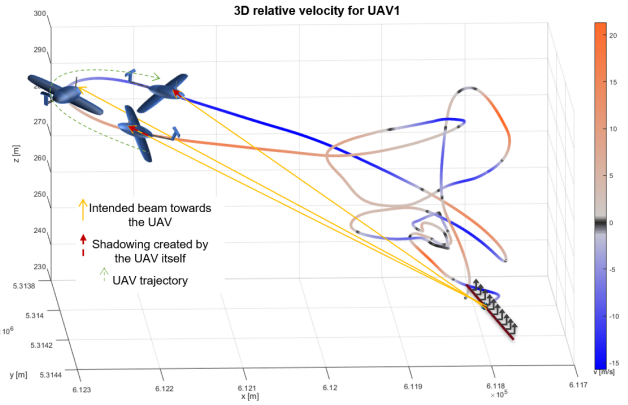

Fig. 7. 3D instantaneous relative velocity and UAV shadowing.

values (shown as green arrows in the bottom plot of Fig. 6), the received power reaches a minimum. On the other hand, a change from positive to negative velocity values (purple arrows) results in a maximum of the received power. Based on that trend, we suspect that there is a minimum around 310 s in the received power for UAV1, as we have a negative to positive zero crossing in the instantaneous velocity at this time. We marked this minimum in the received power with a dotted line and its corresponding green arrow from the relative velocity, with a dashed line to show that they are not based on measured data.

One possible explanation for this correlation between zero crossings in velocity and maxima and minima in the received power is that the UAV itself (along with all the electronics it contains) creates shadowing when changing direction, as its flying inclination is affected. This can be seen in the 3D representation of the instantaneous flying relative velocity of the UAV1 in Fig. 7. When the UAV changes direction, meaning it turns around, it changes its velocity from positive (red) to negative values (blue), or vice versa. The zero crossings are marked in black. As an exemplary case, we show an schematic view of what happens in the most outer turn, where we can assume that the flying inclination of the UAV determines whether it is affected by self-shadowing. In addition, we cannot exclude the effects of a non omni-directional radiation pattern at the antenna mounted on the UAV, which will also be affected by the flying inclination.

V. Conclusion

We presented an electronically adaptable multi-beamformer consisting of a linear array of 10 dipole elements with a transmission frequency of 3.2 GHz and a $\lambda/2$ spacing. We used the linearly constrained minimum variance beamformer to obtain the antenna coefficients (amplitude and phase) that synthesize up to 3 simultaneous beams. These coefficients were stored in a look-up table to preserve a low computational complexity of a hardware implementation and enable a real-time operation, with which several C2 links for UAVs can be electronically tracked. The synthesized radiation patterns for one, two and three rays were validated with real measurements under free space conditions.

In order to simultaneously characterize several C2 links for UAVs, we designed a fully functional system that allowed us to record the received signal at the UAVs using a light-weight SDR module mounted on the UAV. Two tests were carried out with two UAVs operated at the same time. In the first test, two fixed beamforming angles were set and kept constant while the UAVs were moved in different directions. We observed that the received power increased by about 10 dB when the UAV crossed one of the main beams, in agreement with the gain difference between the main beam and the side lobes of the implemented beamformer pattern. In addition, the type of antenna used on the UAV, possible ground reflections and the UAV morphology also influence the strength of the received signal and should be accounted for. In the second test, the beamformer generated the two beams that electronically tracked the two UAVs in real time. In this test, we conclude that the electronics built inside the UAV as well as its flying inclination create self-shadowing and they have a strong influence on the received power and are, therefore, not negligible even in LOS conditions.

Acknowledgment

This work received funding by the MCUAS project supported by the Austrian Austrian Research Promotion Agency (FFG) under the programme FORTE of the Federal Ministry of Finance (BMF) and by the Principal Scientist grant Dependable Wireless 6G Communication Systems (DEDICATE 6G) at the AIT Austrian Institute of Technology.

References

[1] B. Canis, *Unmanned Aircraft Systems (UAS): Commercial Outlook for a New Industry*, report, September 9, 2015; Washington D.C.. (https://digital.library.unt.edu/ark:/67531/metadc770623/: accessed August 24, 2022), University of North Texas Libraries, UNT Digital Library, https://digital.library.unt.edu; crediting UNT Libraries Government Documents Department.

[2] M. Campion, P. Ranganathan, and S. Faruque, *UAV swarm communication and control architectures: a review*, Journal of Unmanned Vehicle Systems, vol.7, num.2, 2019, pp.93-106.

[3] İ. Bekmezci, O. K. Sahingoz, Ş. Temel, *Flying Ad-Hoc Networks (FANETs): A survey*, Ad Hoc Networks, vol.11, Issue 3, 2013, pp. 1254-1270

[4] W. Khawaja, I. Guvenc, D. W. Matolak, U.-C. Fiebig and N. Schneckenburger, *A Survey of Air-to-Ground Propagation Channel Modeling for Unmanned Aerial Vehicles*, in IEEE Communications Surveys Tutorials, vol. 21, no. 3, pp. 2361-2391, thirdquarter 2019.

[5] A.A. Khuwaja, Y. Chen, N. Zhao, M. -S. Alouini and P. Dobbins, *A Survey of Channel Modeling for UAV Communications*, in IEEE Communications Surveys Tutorials, vol. 20, no. 4, pp. 2804-2821, Fourthquarter 2018.

[6] D. W. Matolak, *Air-ground channels models: Comprehensive review and considerations for unmanned aircraft systems*, 2012 IEEE Aerospace Conference, 2012, pp. 1-17.

[7] D. W. Matolak, R. Sun, *Air-ground channels models: Comprehensive review and considerations for unmanned aircraft systems*, in IEEE Vehicular Technology Magazine, vol.10, Issue 2, pp.79-85, 2015.

[8] H.L. Van Trees, *Optimum Array Processing*. New York, NY: Wiley-Interscience, 2002.

[9] D. Löschenbrand, M. Hofer, L. Bernadó, G. Humer, B. Schrenk, S. Zelenbaba, and T. Zemen, *Distributed massive MIMO channel measurements in urban vehicular scenario*, in 13th European Conference on Antennas and Propagation (EuCAP), Krakow, Poland, April 2019.